Numerical simulation of dust-acoustic waves

D. Winske and M. S. Murillo
Applied Theoretical and Computational Physics Division, Los Alamos National Laboratory, Los Alamos, New Mexico 87545

M. Rosenberg
Department of Electrical and Computer Engineering, University of California, San Diego, La Jolla, California 92093

(Received 4 June 1998; revised manuscript received 15 September 1998)

We use molecular dynamics (MD) and particle-in-cell (PIC) simulation methods, in which dust grains are treated as discrete particles and the background plasma is included in the potential shielding (MD) or as a Boltzmann fluid (PIC), to investigate dust-acoustic waves in a one-dimensional, strongly coupled (with the Coulomb coupling parameter Γ equal to the ratio of the Coulomb energy to the thermal energy, which is greater than 1) dusty plasma. We study cases both where the dust is represented by a small number of simulation particles that form into a regular array structure at large Γ (crystal limit) and where the dust is represented by a much larger number of particles (fluid limit). We show that the measured frequency for dust acoustic waves satisfies either a fluidlike dispersion relation or a lattice wavelike dispersion relation, depending on Γ and the number of simulation particles. Other PIC simulations, either with plasma ions represented as particles rather than as a Boltzmann fluid or with collisions between the dust and the background gas, have also been carried out and shown to agree with theoretical predictions. Numerical issues associated with smoothing of the accumulated charge density in PIC simulations have also been addressed; smoothing is shown to affect wave dispersion at high wave numbers in the fluid limit and low wave numbers in the crystal limit.
[S1063-651X(99)01602-5]

PACS number(s): 52.35.Fp, 52.65.Rr, 52.25.Vy

I. INTRODUCTION

When dust grains are introduced into a plasma, they become charged and form a dusty plasma. The environment near a comet and dust rings in planetary magnetospheres are the most common examples of dusty plasmas in space, although they also occur in the ionosphere as well as near the surface of the moon [1–3]. While dusty plasmas have been studied in the context of astrophysics for many years and the effect of electromagnetic fields on dust grains in planetary rings was vigorously investigated a decade ago [4], a more general interest in dusty plasmas has rapidly grown in the past few years. In part, this has been due to laboratory experiments that show a fascinating range of unusual phenomena, including the formation of crystal-like structures and large-amplitude waves [5–9]. Interest has also been generated by the importance of contaminants in industrial processing plasmas [10]. In addition, recent developed computational capabilities and techniques allow these processes to be studied numerically with a high degree of realism that was unavailable just a few years ago.

The presence of charged dust in a plasma adds additional sources of free energy that can modify existing waves or excite new modes [11–13]. High-frequency modes (much greater than frequencies associated with the dust) can be altered because the dust can modify the number of unattached electrons in the system or the relative drift between the plasma electrons and ions. More interesting effects occur at lower frequencies, where the dust dynamics enters directly. Although the dust charge q_d can be large, typically 10^3-10^5 electron charges, and the dust mass m_d is also large ($\sim 10^{12}$ proton masses for a 1-μm-radius spherical grain), so that $q_d/m_d \ll 1$, the dust plasma frequency $\sim q_d/m_d^{1/2}$ can be significant. Both electrostatic and electromagnetic modes exist and many have been studied analytically. One of the most interesting wave modes is the dust-acoustic mode [14,15], which results from the oscillatory motion in a plasma with two species of widely differing masses, in this case dust and plasma ions, rather than ions and electrons. Dust-acoustic waves have been studied in a number of laboratory experiments [7,9,16,17], in which the basic dispersion properties of the waves have been measured. When a relative drift exists between the plasma and the dust, dust-acoustic waves can be driven unstable. Such a situation occurs in the E ring in the inner magnetosphere of Saturn [18,19], where the plasma corotates with the planet while the dust follows Kepler orbits. The relative drift speed between the plasma and the dust is of the order of the ion thermal speed, which is sufficient to drive the instability.

In the past few years, it has been shown experimentally that dust grains in a plasma can form into a regular crystalline lattice [5,6,8]. By adjusting the parameters of the plasma the plasma crystal can be changed into a liquid or a gaseous state. It has been known for many years that coulomb systems can exist in a solid state when the coupling parameter Γ, the ratio of the Coulomb energy to the thermal energy, exceeds ~ 170; such processes have been investigated in colloidal systems and non-neutral plasmas (see, e.g., [20]). Since the charge on a dust grain can be very large, it is possible achieve dusty plasmas with $\Gamma \sim 10^3-10^5$. The plasma crystal is easily observed with a scanning laser and a video camera and forms in a few seconds. Dust-acoustic waves can be excited in these systems by applying a small voltage pulse to a probe in the plasma. The characteristics of the waves can be used to determine properties of the dust grains, such as their charge and screening length [16] and

 ©1999 The American Physical Society

even perhaps their size [21]. Low-frequency waves in a regular crystal array may exhibit dispersion properties that depend on the lattice [22,23], in analogy to solid state physics; however, the measured wave properties in plasma crystals seem to correspond more closely to those obtained from simple fluid theory [16]. Enhanced fluctuations are also associated with the melting of the crystal [8,24,25]. In addition, strongly coupled plasma effects may occur in these crystals [26,27], although they do not appear to be significant in present experiments.

In this paper we describe simulation models for studying dust-acoustic waves and results of calculations. As described previously, there is general interest in the properties of the waves in both the fluid limit, where the dust is continuously distributed, and the crystalline phase, where the dust consists of a few large grains collected into a regular lattice. Because the lattice forms in rf discharge plasmas near the outer edge of the sheath above the electrode, the flow of plasma ions into the sheath through the lattice can also be important and may contribute to the structure of the crystal that is formed [28] as well as to the spectrum of low-frequency fluctuations. Moreover, the possible existence of lattice vibrations and strongly coupled effects in such configurations is also of interest. Simulations allow the properties of the waves to be studied in the absence of complicated effects, such as variable grain charge, spatial inhomogeneities, and boundary effects, although such effects could be addressed by calculations in the future.

Since the background plasma primarily provides shielding, the most straightforward simulation model is molecular dynamics (MD) that calculates directly the interaction of N_d dust grains with fixed charge and mass [29–32]. Each grain is characterized by a screened Coulomb (Yukawa) potential, which takes into account the effects of the plasma. The MD approach allows the grains to interact at distances shorter than a Debye length. Hence strongly coupled plasma and lattice effects at short wavelength can also be included directly. An alternative approach is to again treat the grains as discrete particles, but use a grid to compute the fields that the particles experience. In this particle-in-cell (PIC) method, the plasma electrons and ions are treated as a Boltzmann fluid at constant temperature [33]. One simulates this system in the usual manner, using PIC methods for the grain dynamics and solving Poisson's equation to obtain the electric field [34]. If one wants to model more complex situations, such as including the effect of flowing ions, the shielding of each grain needs to be modified. In the MD model, this can be done by changing the form of the potential when one grain is located downstream of a second grain. For example, Melandso and Goree [28] have added a dipole force to model this interaction. In the PIC approach, the modification to include the effects of plasma flow is less clear. The easiest (but most expensive) approach is to represent the plasma ions by PIC methods as well [19,35].

Each of these numerical methods has its strengths and weaknesses. For studying the generation and properties of dust-acoustic waves, one technique may be more appropriate in certain regimes than others. In addition, the underlying assumptions of the physical model and/or the numerical method used in its implementation may add further constraints. Additional conditions on the usefulness of a particular approach may be imposed by other physics dictated by the experimental conditions, such as collisional coupling to the background gas and plasma as well as boundary conditions. While these sorts of issues for studying waves using plasma simulation techniques are fairly well known in ordinary collisionless plasmas (see, e.g., [34]), dusty plasmas add new complications, as described previously.

While our eventual goal is the study of dust-acoustic-like fluctuations in laboratory experiments, we realize the need to start at a fairly elementary level and address some of the most fundamental issues first. Thus we concentrate on one-dimensional systems in which the dust is considered either as very fine grains, which can be modeled as a fluid, or as massive grains, as one finds in a plasma crystal. We begin in Sec. II with a brief review of the theory of dust-acoustic waves in these two limits and include the effects of lattice vibrations, strong coupling, and collisions. In Sec. III we review the numerical techniques we will employ: MD techniques and PIC methods for the dust ions, with the plasma ions treated either as a Boltzmann fluid or as PIC particles. The results of various simulations are presented in Sec. IV, where we discuss both the physics of the simulations and the limitations imposed by the numerics. Results for the various methods will be compared and contrasted. The findings of this study are summarized in Sec. V and remaining issues are discussed.

II. THEORY

We consider low-frequency electrostatic waves in a dusty plasma. The plasma is characterized by ions of number density n_i, charge $Z_i e$, mass m_i, and temperature $T_i = \frac{1}{2} m_i v_i^2$ and electrons of density n_e, mass m_e, charge $-e$, and temperature $T_e = \frac{1}{2} m_e v_e^2$. The dust grains are all assumed to be the same size (spherical with radius a), with mass m_d, charge $q_d = Z_d e$ (usually less than 0), and temperature T_d. The dust charge density n_d then relates the electron and ion densities through the condition of charge neutrality

$$Z_i n_i - n_e + Z_d n_d = 0. \tag{1}$$

The dispersion relation relating the frequency of the waves ω to the wave number k for dust-acoustic waves is readily obtained by linearizing and combining the continuity and momentum equations for all three species in standard fashion [14,15,18] to obtain

$$\omega = \omega_d \frac{k/k_D}{(1 + k^2/k_D^2)^{1/2}}, \tag{2}$$

where the dust plasma frequency is $\omega_d = (4\pi n_d Z_d^2 e^2/m_d)^{1/2}$ and $k_D = \lambda_D^{-1} = (\lambda_{\mathrm{De}}^{-2} + \lambda_{\mathrm{Di}}^{-2})^{1/2}$, where $\lambda_{D\alpha} = (T_\alpha/4\pi n_\alpha Z_\alpha^2 e^2)^{1/2}$ is the Debye length for the αth species. When $T_e \sim T_i$ and $n_e \sim n_i$, $\lambda_D \sim \lambda_{\mathrm{De}}$ while for $T_e \gg T_i$, which will be valid for most of the results presented in this paper, $\lambda_D \sim \lambda_{\mathrm{Di}}$.

The dispersion relation (2) is modified by several effects that are important in various applications of dust-acoustic waves. First, dust-acoustic waves are often observed in dusty plasma crystals. The presence of dust-acoustic fluctuations can be related to the periodicity of the lattice and seem to be

associated with the melting of the crystal [8,24]. Dust-acoustic-like lattice waves have been analyzed using well known techniques from solid state physics [24,36]. In this case, the dispersion relation takes the form

$$\omega = \omega_d f(k_D b)\sin(kb/2), \tag{3}$$

where

$$f(k_D b) = C(1 + k_D b + k_D^2 b^2/2)^{1/2} \exp(-k_D b/2). \tag{4}$$

$C = \pi^{-1/2}$ and b is the spacing between grains in the lattice.

Strongly coupled plasma effects may also occur in dusty plasma. Such effects are characterized by the Coulomb coupling parameter

$$\Gamma = \frac{Z_d^2 e^2 \exp(-d/2\lambda_D)}{(d/2)k_B T_d}, \tag{5}$$

where $d/2$ is the Wigner-Seitz radius. Strictly speaking, strong coupling has not been worked out for a one-dimensional system. So here we take the Wigner-Seitz radius to be half the intergrain spacing in a cubic lattice, $d = (1/n_d)^{1/3}$, and k_B is the Boltzmann constant. (Note that here we distinguish between d, the average spacing between grains that can be positioned at random, and b, the separation between grains equally spaced in an array. The first quantity is most relevant when a fluid description is being used, whereas the second quantity is significant when lattice dynamics are important.) Strong coupling ($\Gamma > 1$) can occur in these systems since the dust charge can be very large. For large Γ [>170 for three-dimensional (3D) systems, >120 for 2D systems) strong coupling effects can be manifested in the formation of crystallinelike structures in the dust [6,8].

Strong coupling effects in dusty plasmas have recently been considered theoretically by Rosenberg and Kalman [26] and Murillo [27]. An approximate expression for the dispersion relation in this limit is given by Murillo:

$$\omega = \omega_d \frac{k/k_D}{(1 + k^2/k_D^2)^{1/2}} \frac{1}{(1 + k^2 d^2/16)^{1/2}}. \tag{6}$$

This expression does not depend explicitly on Γ; it is an average fit for a range of different Γ's. A more complete expression is given in Eq. (34) of Ref. [26], which is valid in the liquid phase at long wavelengths (for $\kappa = d/\lambda_D \leqslant 1$), and is of the form

$$\omega = \omega_d \frac{k}{k_D}\left[\frac{1}{(1 + k^2/k_D^2)} + f(\kappa,\Gamma)\right]^{1/2}, \tag{7}$$

where f is a complicated function of κ and Γ, given by Eq. (35) of [26]. Both models show that the effect of strong coupling is to reduce ω at short wavelengths, so that the phase velocity is negative. For the range of wave numbers of interest here, the dispersion ($\partial\omega/\partial k$) approaches zero, but does not become strongly negative, as can occur at shorter wavelengths. The more comprehensive model [26] includes strong coupling effects on the plasma compressibility, which results in a reduction of the phase speed at long wavelengths, as shown later.

A third modification involves the inclusion of collisions between the plasma species and the background neutral species. In the cold fluid limit, the left-hand side of Eq. (2) is replaced with $[\omega'(\omega' + i\nu_c)]^{1/2}$, where ν_c represents collision of dust or plasma ions with the neutral species [16,37,38]. In the collisionless case, the fluid damping rate of the waves γ is zero. With collisions, the complex frequency ω' goes to $\omega - i\nu_c/2$, so the damping rate is increased to $\nu_c/2$. Also, the left-hand side goes to $(\omega^2 + \nu_c^2/4)^{1/2}$ and hence the real frequency is reduced. For finite temperature, the dispersion equation must be solved numerically, as discussed later.

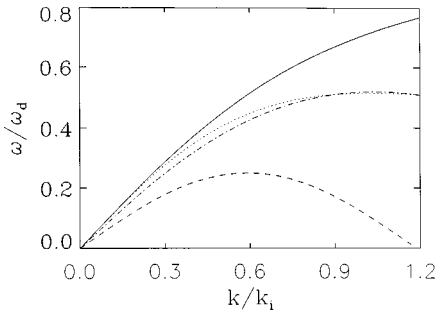

FIG. 1. Real frequency ω, normalized to the dust plasma frequency ω_d, versus wave number k, normalized to the inverse ion Debye length k_i, as computed from fluid theory [Eq. (2)] (solid curve), fluid theory with strongly coupled correction [Eq. (6)] (dotted curve), fluid theory with strongly coupled correction [Eq. (7)] (dot-dashed curve), and lattice dynamics [Eq. (3)] (dashed curve). The parameters are given in the text.

A fourth effect (which we will not consider, but discuss briefly for completeness) is the relative drift between the dust ions and the plasma. As noted earlier, such a relative drift can arise in planetary rings. A similar drift also occurs in many laboratory discharges, either by directly inducing it [7] or naturally by the plasma flows in the sheath region of rf discharges where dusty crystals tend to form. The presence of the drift allows the dust-acoustic waves to become unstable and hence grow to large amplitude from background fluctuations. While analytical expressions can be obtained for the growth rate γ in the limit of relatively small or very large ion drifts [18], in general, one needs to solve the dispersion relation numerically when the drift is comparable to the ion thermal velocity (see, e.g., [19,39]).

To show how these effects modify the dispersion relation in a quantitative manner, we consider a set of specific parameters, which are roughly based on typical experimental conditions in rf discharges, which will be used throughout the study. Using ion quantities as normalization, with $Z_i = 1$, we assume $n_d/n_i = 10^{-4}$, $Z_b = -2000$, $T_d/T_i = 1$, and $m_d/m_i = 10^{12}$. This further implies that $n_e/n_i = 0.8$ and, assuming $T_e/T_i = 40$, $k_D \sim \lambda_{\mathrm{Di}}^{-1} = k_i$. Using $n_d d^3 = 1$ implies a particle spacing d of $k_i d = 5.3$. For the above parameters, one finds the coupling parameter [Eq. (5)] $\Gamma \sim 120$ for $T_d/T_i = 1$. We will also show simulation results at smaller Γ by reducing the dust temperature. For a few of the calculations, an artificially small dust mass $m_d/m_i = 10^6$ is used instead. This is needed when the motion of the plasma ions is explicitly included.

With these parameters, the dispersion relation including the various additional effects can be plotted. Equation (2) for these parameters is plotted in Fig. 1 as a solid line. The real

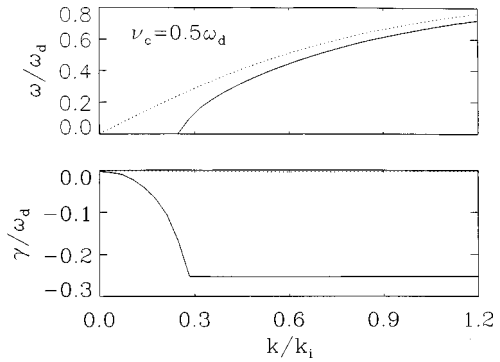

FIG. 2. Numerical solution of the dispersion equation including collisions between dust and background gas ($\nu_c=0.5\omega_d$), showing ω versus k (top panel) and damping rate γ versus k (bottom panel); the dotted curve is the collisionless result for comparison. The parameters are the same as in Fig. 1.

frequency ω is linear at small k and bends over as k approaches unity. Superimposed on the figure is the dispersion relation modified by the lattice [Eq. (3), dashed line] with $b=d$ and strongly coupled effects [Eq. (6), dotted line; Eq. (7), dot-dashed line]. At short wavelengths, the strongly coupled effects in both models lead to a comparable reduction of the frequency. The reduction increases with Γ. At long wavelengths, Eq. (6) reduces to the fluid limit (2), while the more complete model (7) gives a reduction in the phase speed that also increases with Γ; for $\Gamma\sim 100$, this reduction is about 10%. Lattice effects lead to a larger reduction of the frequency compared to the fluid case; for short wavelengths where $kb>\pi$ $(k/k_i=0.6)$, the wave dispersion becomes negative.

Figure 2 shows the effect of including collisions between the dust grains and the background gas. Again, the real and imaginary parts of the frequency are solved numerically [Eq. (2) in [40]], using the same parameters as above, with the dust-neutral collision frequency $\nu_d=0.5\omega_d$. We have also plotted the numerical solution for $\nu_d=0$ for comparison as the dotted lines. Including collisions tends to reduce the real frequency of the waves compared to the collisionless case and increase the wave damping by about $\nu_d/2$. At small k, the real frequency is reduced to approximately zero and the damping rate decreases with wave number. In the absence of collisions, the kinetic wave damping rate is very small ($<1\%$ of ω_d).

The results displayed in Figs. 1 and 2, which use parameters that are characteristic of many laboratory experiments, indicate both numerical and experimental challenges of inferring plasma properties of the plasma and dust from dust-acoustic waves. We note from Fig. 1 that the difference between the fluid dispersion relation and corrections imposed by the lattice or strongly coupling are relatively small at long wavelengths and become sizable only at short wavelengths. The modification to the wave dispersion due to collisional effects are likely to complicate the interpretation of these corrections [16,26]. In addition, the presence of plasma flow (which we do not consider in this paper) can also modify the dispersion. In a realistic 3D dusty plasma crystal, the flow will be primarily in one direction (normal to the electrode) and the driven oscillations in this direction will likely couple to other modes in the transverse directions as well. These complications are beyond the scope of this study. As we will show in Sec. IV, numerical issues can add further complexities to interpreting the results in the calculations.

III. METHODOLOGY

In this section we review the numerical methods that we will use to simulate dust-acoustic waves. We also discuss the initial conditions of the simulations as well as method used to model collisional coupling to the weakly ionized, background plasma. The techniques that are used to construct the dispersion relation are also described.

As discussed briefly in the Introduction, we employ both PIC and MD methods. MD methods are conceptually simpler, in that one computes directly the two-body interactions between N_d charged dust grains. By including all the interactions, one treats both short-range and long-range interactions identically. The effect of the background plasma is included as the shielding around each of the grains, with the potential surrounding each particle assumed to be a shielded Coulomb (Yukawa) potential, i.e.,

$$\phi(x)=\frac{Z_d e}{x}\exp(-x/\lambda_D). \tag{8}$$

Each dust particle has mass m_d and charge $Z_d e$ and is characterized by its velocity v_i and position x_i. The equations of motion for the ith particle are

$$m_d\frac{dv_i}{dt}=-\sum_{j\neq i} Z_d e\left.\frac{d\phi(|x-x_j|)}{dx}\right|_{x=x_i},$$
$$\frac{dx_i}{dt}=v_i, \tag{9}$$

where the sum is over the other dust particles. As described later, the calculations are done in a periodic system, which implies that the sum must be done not only over the simulation particles in the actual system but also over their counterparts in periodic replications of the system. However, because of Debye shielding, in practice we need only worry about particles that are located within $\pm L/2$ of the ith particle.

Other effects that can occur in a realistic experiment can also be included by augmenting the grain-grain interactions with an external potential that models the effects of the electrical force due to an imposed electric field at the boundary and the gravitational force [30,32]. In addition, the effect of the interaction with the background plasma can be included through an imposed cooling of the grains or through the addition of a short-range force to model neutral-dust collisions [41]. By suitably modifying the potential structure, wakes due to flowing plasma can also be readily incorporated [28].

MD simulations generally are characterized by rather high noise levels due to the short-range interactions. In addition, because of the need to resolve each grain-grain interaction, the time step is relatively small. Increasing the particle number decreases the intergrain particle spacing and thus leads to small time steps and longer computer runs. This is offset by the ability to model short-range interactions self-consistently and the simplicity of extending the calculations to three di-

mensions. For doing complex problems, there are sophisticated methods available to make MD more efficient [29], but for the one-dimensional calculations to be presented here, they are not necessary.

While direct, MD-like methods were used in the early days of numerical simulation of collisionless plasmas; PIC methods replaced them in the early 1970s. In the PIC method, the electromagnetic fields that the particles experience are stored on a grid. The field information at the grid points located on either side of each particle is interpolated to the particle position to determine the instantaneous force by which the particle is advanced to the next time level. After the particles are moved, their charges and currents are interpolated back onto the grid. Using these source terms, the electromagnetic fields are then solved on the grid. In this case, the equations of motion are

$$m_d \frac{dv_i}{dt} = -Z_d e \left. \frac{d\phi(x)}{dx} \right|_{x=x_i}, \qquad \frac{dx_i}{dt} = v_i, \tag{10}$$

where the electrostatic potential ϕ obeys Poisson's equation

$$\frac{d^2\phi(x)}{dx^2} - k_D^2 \phi(x) = -4\pi Z_d e[n_d(x) - n_{d0}], \tag{11}$$

with the background plasma included as a correction to the linear dielectric. n_{d0} is the spatial average of $n_d(x)$. $\phi(x)$ and $n_d(x)$ are calculated on a fixed grid of N cells, at positions $x_k = (k-1/2)L/N$, $k = 1,2,\ldots,N$, as described in Chap. 2 of Ref. [34]. This method of interpolation between particles and the grid has the advantage that short-range interactions are smeared out, reducing the level of fluctuations considerably. As is typically done, it is assumed here that the particle size corresponds to the cell size and linear interpolation is used both in collecting the source terms and in determining the electric field experienced by each particle (see, e.g., Ref. [34], pp. 19–22). This means that the electric field experienced by the grains in a cell is just a linear function of their position in the cell. Further reduction of the short-range forces occurs because of additional smoothing that can be applied to the source terms when the solving the field equations. The additional smoothing retains the linear nature of the force experienced by a particle, but reduces the cell to cell variations. Long-range interactions are essentially similar to the MD approach. However, one can show that PIC methods require only $N_d \log N_d$ computations per time step, compared to N_d^2 for MD. In the case of the PIC method, one can use only a few simulation particles to represent the large grains in a dusty plasma crystal or many simulation particles to represent a quasicontinuum of dust grains as would be described by fluid theory. However, calculations in more than one spatial dimension require some effort to solve the field equations. In the calculations to follow, we consider only electrostatic interactions and hence just solve Poisson's equation. We assume that all the dust grains have identical, fixed charges, but one could also imagine allowing the grain charge to vary in time or having a distribution of charges/sizes [19].

In the simplest PIC simulations, the background plasma ions and electrons are modeled as a Boltzmann fluid, which enters into the solution of Poisson's equation. In some simulations, we will instead treat the background ions, like the dust grains, as simulation particles. This has the advantage that the ion interactions are all self-consistent and is most useful for more complex problems, such as those involving ion flow. However, it implies that one must follow the plasma ions as well as the dust. Because of the highly disparate time scales between dust and plasma ions, we use an artificially small dust mass ($m_d/m_p = 10^6$ rather than $m_d/m_p \sim 10^{12}$ for a 1-μm dust grain). PIC simulations with particle dust grains and plasma ions have been used to study short-range correlations [35] as well the dust-acoustic instability in a flowing plasma with [40] and without [19] collisions with the background gas. Simulations with PIC ions and electrons have been done to study grain charging in a self-consistent manner [42,43].

The PIC and MD simulations carried out in this study have been initialized in the same manner. Particles are placed in the simulation domain at equally spaced positions and given random thermal velocities. Periodic boundary conditions are used for particle motion and the electrostatic potential (electric field) in both methods. In both types of calculations, local fluctuations develop and the particles acquire random displacements from these positions, resulting eventually in some heating of the dust. In most calculations, this heating does not affect the overall results. In order to verify this, in some calculations the dust temperature was fixed by renormalizing the velocities of the dust grains each time step to ensure that the temperature is truly constant [44]. Alternatively, a collision operator is turned on to cool off the particles to a prescribed temperature for some time (usually $\omega_d t = 50$). This is done using the Langevin approach we have developed for semicollisional plasmas [45] and have applied to collisional dusty plasmas [40]. After moving the particles, the velocity of each particle v_i is subject to collisions with the background plasma (ν_c), according to the Langevin equation [44]

$$\frac{dv_i}{dt} = -\nu_c v_i + v_{\rm th}\sqrt{2\nu_c t}R, \tag{12}$$

where R is a random number and $v_{\rm th}$ is the thermal velocity. This has the effect of collisionally slowing and cooling (or heating) the grains to the velocity and temperature of the background. This process produces some small fluctuations in the temperature of the dust grains. We also apply the approach in Eq. (12) continuously through the run to treat the effect of collisions with the background gas, as discussed earlier in regard to Fig. 2.

In all of the simulations, we use a similar time step $\omega_d \Delta t = 0.05$. The simulations are run (after the initial randomization and cooling period of $100\omega_d^{-1}$) for $410\omega_d^{-1}$, during which time (8192 time steps) we collect the electrostatic potential on the grid. The grid consists of 128 equally spaced positions for a system length of $Lk_i = 85$. In the case of the MD simulations, where no potential profile or even a grid is needed, we calculate the potential on a fictitious grid (i.e., on fictitious particles with fixed spatial locations) in the same manner as for the PIC simulations. We then Fourier trans-

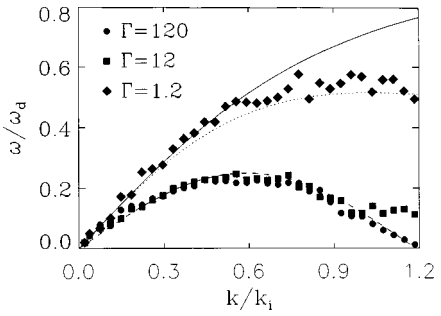

FIG. 3. ω versus k from MD simulations with $N_d=32$ and $\Gamma=120$ (circles), 12 (squares), and 1.2 (diamonds). Curves in this and subsequent figures are the theoretical results from Fig. 1.

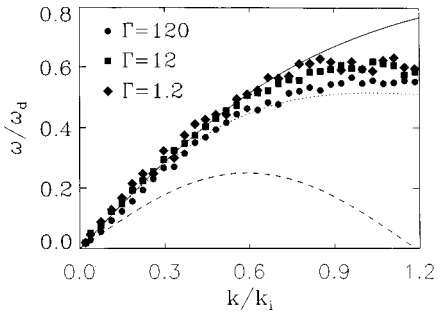

FIG. 4. ω versus k from PIC simulations with $N_d=12\,800$ and $\Gamma=120$ (circles), 12 (squares), and 1.2 (diamonds).

form the data in space and time. For each wave number, we obtain a spectrum of frequencies. From suitable wave-power averaged frequencies, we compute a mean frequency ω for each wave number k. The spread of frequencies about the mean is typically ~5%. We will show plots of the dispersion relation ω versus k for the various runs we present in Sec. IV. Experimentally, one usually launches waves of fixed frequency and measures the (complex) wave number. Our later studies will consider such launched waves and the resulting spatial damping effects.

Finally, we will consider two limiting cases. To model dusty crystal-like structures in both MD and PIC simulations, we use 32 particles in the simulation. For the parameters given above, this corresponds to a particle spacing b of about one electron Debye length (five ion Debye lengths), with $b=d=n_d^{-1/3}$. In the PIC simulations, this corresponds to about one particle every four computational cells. For the PIC calculations, we will also consider the fluid limit, where discreteness effects usually associated with dust grains are ignored; here the dust is presented by roughly 100 particles per cell. In this case, the particle number is so large and the interparticle spacing is so small that MD methods are impractical.

IV. SIMULATIONS

In this section we present the results from a number of different simulations, comparing the dispersion relation for dust-acoustic waves for different physical or numerical parameters. We begin with MD simulations for a plasma crystal containing 32 dust grains. The physical parameters have been all given in the preceding section. We consider three cases, in which the dust temperature is varied, so that Γ is 120, 12, or 1.2. The results are shown in Fig. 3, in a format used in subsequent plots. Plotted as curves in the figure are the fluid dispersion relation (2) as the solid curve, the fluid dispersion relation with strongly coupled corrections (6) as the dotted line, and the dispersion relation appropriate for a 1D lattice (3) as the dashed line. The symbols represent the real frequency ω as a function of wave number k for the various simulations. The circles correspond to the run with $\Gamma=120$. In this case, one finds from the calculations that a regular crystal structure forms. The points correspond rather closely to the dispersion relation predicted by the lattice theory [23], with the frequency dropping to near zero at $k/k_i=1.2$, corresponding to $kb=2\pi$. (With a finer spatial grid, one can show that the sinusoidal pattern repeats at higher wave numbers.) The squares correspond to the run at smaller $\Gamma=12$. In this case, one expects a more liquid behavior, with the frequency falling, but not going to zero, at $kb=2\pi$. The third case (diamonds) corresponds to $\Gamma=1.2$. In this case, one expects the grains to be in a gaseous state, obeying a more fluidlike dispersion relation. For $k/k_i>0.6$, the points lie above, but more closely to, the dotted curve, which is the strongly coupled modification to the fluid dispersion relation [27]. At long wavelengths $k/k_i<0.6$, strongly coupling effects at large Γ are negligible and the points follow the solid curve, the fluid relation (2).

We now contrast these results with different simulations done with PIC techniques. We begin in Fig. 4, with simulations in the fluid regime, where the dust is represented by 100 macroparticles per computational cell (i.e., 12 800 total particles). In this case, one expects that discrete effects will be negligible and that one should recover the wave properties obtained from the fluid equations. Again, we consider three cases: $\Gamma=120$ (circles), 12 (squares), and 1.2 (diamonds) and display the results in Fig. 4 in the same format as Fig. 3. At short wavelengths, the strongly coupled case ($\Gamma=120$) more closely follows the dotted curve (6). As Γ is reduced, the frequencies follow the fluid dispersion relation to higher k, before leveling off. At long wavelengths, the points corresponding to the cases at higher Γ generally fall below those at low Γ. A least-squares (linear) fit to the five smallest k values yields phase speeds relative to the fluid limit ($=1.0$) of 1.1 ± 0.05 at $\Gamma=1$, 1.0 ± 0.05 at $\Gamma=12$, and 0.9 ± 0.05 at $\Gamma=120$. The reduction in phase speed with Γ is consistent with theory [26], although calculations have not been done explicitly for these parameters in a 1D model. The theory, derived for $\kappa=d/\lambda_D<1$, has not been extended to the regime $\kappa>1$ ($\kappa\sim5$ in the simulations). Moreover, differences to the strong coupling correction to the compressibility between the 3D theory and the 1D simulations have not yet been worked out.

In order to test the sensitivity of these PIC results to numerical effects, we consider the $\Gamma=120$ case, but vary the way that the dust density information that is collected on the spatial grid is treated. These results are presented in Fig. 5. The circles correspond to the same case as shown in Fig. 4, where no numerical smoothing is applied to the collected density, which is used to solve Poisson's equation. The squares correspond to a run where we apply a simple smoothing routine, in which the charge density in the jth cell is taken to be a weighted average of the values in the (j

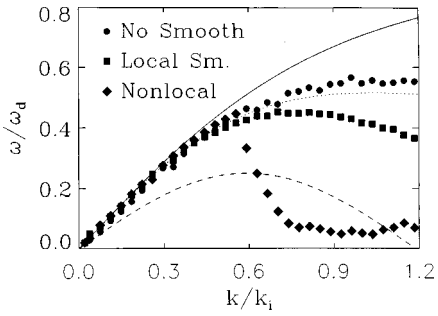

FIG. 5. ω versus k from PIC simulations with $N_d = 12\,800$ and $\Gamma = 120$ for no smoothing (circles), simple local smoothing (squares), and nonlinear smoothing (diamonds).

$-1)$th (25%), the jth (50%), and the $(j+1)$th (25%) cells. With this simple smoothing routine, one sees similar results at long wavelength but a reduction of the frequency for $k/k_i > 0.6$, which corresponds to wave modes that are resolved by fewer than eight cells. The diamonds correspond to the results of a third simulation in which a stronger, nonlinear filter is applied. This filter is applied by Fourier transforming the accumulated charge density into k space, reducing the wave power in waves with mode number greater than 16 (i.e., waves resolved by fewer than eight cells) exponentially, and transforming the truncated spectrum back to real space. As one sees in the figure, the spectrum is well represented by the fluid dispersion relation below this cutoff, but for high wave numbers, the frequency is strongly reduced. This shows that the PIC methods with smoothed density profiles are valid at long wavelengths, but care must be used in interpreting results at shorter wavelengths.

Figure 6 shows how the dispersion relation for the (unsmoothed) PIC simulations varies as the particle number is reduced. Again, the dust temperature is low, corresponding to $\Gamma = 120$. Plotted as the circles is a run with $N_d = 128$, i.e., one simulation particle per cell. This result is nearly identical to that in Figs. 4 and 5 (again as circles) where $N_d = 12\,800$. One can show that the results are essentially identical for N_d varying between these two limiting values. The second case, shown as squares, corresponds to $N_d = 64$, i.e., one particle for every two cells. In this case again, the fluid dispersion relation continues to be obeyed, even though one might imagine that discrete effects would begin to appear. According to Eq. (3), the lattice dispersion equation expected

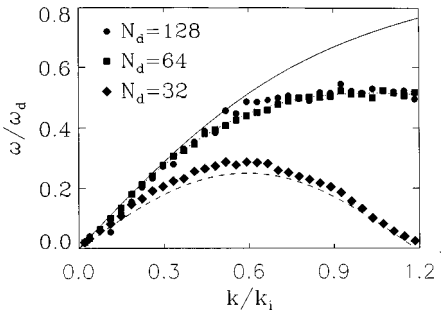

FIG. 6. ω versus k from (unsmoothed) PIC simulations with $\Gamma = 120$ and $N_d = 128$ (circles) (corresponding to one particle per cell), 64 (squares) (0.5 particles per cell), and 32 (diamonds) (0.25 particles per cell).

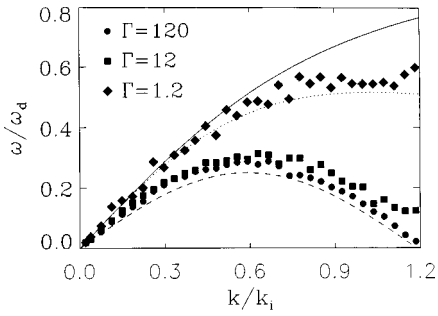

FIG. 7. ω versus k from (unsmoothed) PIC simulations with $N_d = 32$ and $\Gamma = 120$ (circles), 12 (squares), and 1.2 (diamonds).

for 64 equally spaced particles would be a sine function that reaches its first maximum at $k/k_i = 1.2$, with an amplitude of $\omega/\omega_d = 0.4$, which is considerably different from that which is found. Discrete effects do become manifest at $N_d = 32$, i.e., one particle every four cells. In this case, with the measured frequencies shown as diamonds, the dispersion relation obeys the lattice dispersion relation (3), with the frequency peaking at $k/k_i = 0.6$ and falling to zero at $k/k_i = 1.2$, as in Fig. 3.

The results of PIC simulations with $N_d = 32$, corresponding to the crystal state, are shown in Fig. 7, where the dust temperature is varied. Again, the simulations are not smoothed in space and the three cases $\Gamma = 120$ (circles), 12 (squares), and 1.2 (diamonds) can be directly compared to the MD results (which use the same number of particles) in Fig. 3. One sees in comparing these figures that they are very similar, showing solid (lattice) behavior at the highest Γ, more liquid behavior at the intermediate Γ, and fluid-like behavior at $\Gamma = 1.2$. In the present simulations, the frequency for the lattice waves is slightly larger than the theoretical value (and the value obtained in the MD calculations). Because of the sharing of charge between gird points, this suggests that the average effective particle spacing b is slightly smaller than L/N_d, so that from Eq. (4), kb is slightly less. Hence $f(k_D b)$, and thus ω, is slightly larger. This conjecture has been confirmed by redoing the simulations using a nearest grid point method of charge accumulation instead of distributing the charge between the two neighboring grid points [34]. In this case, the frequencies indeed are slightly ($\sim$5%) smaller.

We have also carried out smoothing tests in the crystal limit, as summarized in Fig. 8. As in Fig. 5, we compare PIC

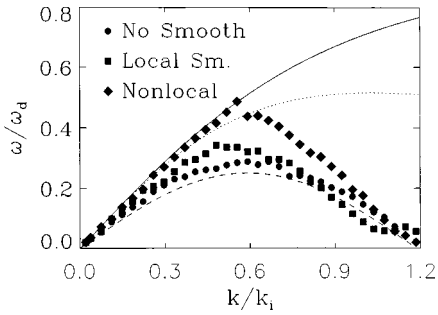

FIG. 8. ω versus k from PIC simulations with $N_d = 32$ and $\Gamma = 120$ for no smoothing (circles), simple local smoothing (squares), and nonlinear smoothing (diamonds).

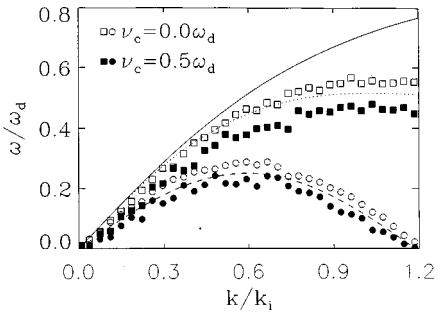

FIG. 9. ω versus k from (unsmoothed) PIC simulations including dust-background collisions ($\nu_c=0.5\omega_d$) for $\Gamma=120$ and $N_d=32$ (filled circles) and 12 800 (filled squares); open symbols are for the corresponding cases without collisions.

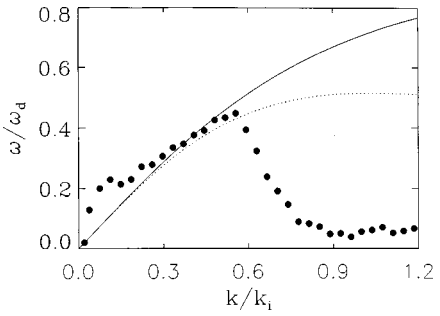

FIG. 10. ω versus k from PIC simulations with particle plasma ions ($N_p=51\,200$) and $N_d=12\,800$.

simulations with no smoothing (circles), simple $\frac{1}{4}$-$\frac{1}{2}$-$\frac{1}{4}$ smoothing (squares), and the more complex filter routine (diamonds), with $N_d=32$ and $\Gamma=120$. The case with no smoothing was shown in Fig. 7. With simple smoothing, the latticelike dispersion relation is still obeyed, but the frequencies of longer-wavelength modes ($k/k_i<0.6$) are increased to values intermediate between the lattice and fluid limits. The more complex, nonlinear filter causes these long-wavelength modes to satisfy the fluid dispersion equation (2) since the smoothing tends to remove discrete effects associated with the small number of grains. At shorter wavelengths, the frequency is reduced, so that ω is nearly zero at $kb=2\pi$, similar to the unsmoothed case.

We have also included collisions of dust grains with the background gas, as described in Sec. III. We compare the previous unsmoothed PIC simulations with $\Gamma=120$ and $N_d=12\,800$ (open circles) and $N_d=32$ (open squares), with corresponding runs where $\nu_c=0.5\omega_d$ (closed symbols), as shown in Fig. 9. As predicted by linear theory (Fig. 2), in both the fluid and crystal limits, the frequency of the waves is reduced, although the general shape of the dispersion relation is relatively unchanged. The percentage reduction of the frequency in each case is consistent with that calculated from linear theory. At long wavelengths, we find a small reduction of the frequency, rather than $\omega\rightarrow 0$, as Fig. 2 indicates. Although the linear damping rates in Fig. 2 are large, the waves are not completely damped out. A comparison of the fluctuation levels in the two fluid regime runs shows that with collisions, the fluctuation levels are about a factor of 10 lower compared to the collisionless case [46]. Whereas in the case of no collisions there is a very slow rise of the fluctuations with time, in the presence of strong collisions, the fluctuations stay clamped at their lower, thermal level throughout the run.

Finally, we have carried out PIC simulations in which the plasma ions are also treated as particles rather than as a Boltzmann fluid. There are 100 dust simulation particles per cell along with 400 plasma simulation particles. In this case, as shown in Fig. 10, the nonlinear smoothing is employed. As in Fig. 5, the waves tend to follow the fluid dispersion curve up to $k/k_i=0.6$, when the nonlinear filter kicks in and reduces the wave frequencies for shorter wavelengths. At long wavelengths, there is some enhancement of the frequency. This may be a nonlinear effect, due to mode coupling because of the much larger noise levels in these simulations (a factor of 100 larger compared to the run that uses Boltzmann ions).

V. SUMMARY

In this paper we have discussed the use of molecular dynamics and particle-in-cell techniques in modeling low-frequency wave behavior in dusty plasmas. We have used these techniques to model dusty plasmas both in the limit where discreteness effects of the dust can be ignored and the resulting system can be described by fluid equations and in the limit where the dust grains are large and form into a regular, latticelike array. In this second, so-called crystal regime, we have shown that MD methods are able to accurately simulate lattice waves when the dust is relatively cold and the coupling parameter Γ is large enough that the solid state is achieved. Moreover, at smaller values of the coupling parameter, both liquid and gaseous (including strong coupling corrections) states can be simulated, as reflected in the accurate representation of the dispersion relation of dust-acoustic-like waves. As one includes all the two-body interactions between grains in this method, MD simulations work best when the particle number is relatively small.

On the other hand, PIC methods, which treat the grain-grain interactions indirectly through the medium of a grid on which moments are collected and the field equations are solved, have been shown to accurately model dusty plasmas in the absence of discreteness effects, i.e., the fluid regime. Some care must be used if smoothing of the moments is applied in order to reduce the fluctuations in the system. Because of smoothing, the short-wavelength portion of the wave spectrum will probably not be properly represented; however, the long-wavelength portion of the spectrum will be accurately reproduced. In the absence of smoothing, PIC methods have been shown to reproduce the fluid dispersion relation modified by strongly coupled plasma effects both at short wavelengths (where the effect is large) and at long wavelengths (where the effect is smaller). The crystal limit can also be modeled by PIC methods, but again smoothing is an issue. In this limit, smoothing can modify the long-wavelength portion of the spectrum and make the dispersion more fluidlike rather than latticelike. In the absence of smoothing, the lattice dispersion relation is generated whenever there are sufficiently few particles (e.g., about one particle every four cells) that discreteness effects appear. In this limit, with relatively few particles, PIC methods are about as computationally efficient, and somewhat less accurate for

doing short-range interactions, than MD methods. This will be particularly true in more than one spatial dimension.

We have also shown how collisions between grains and the background plasma and/or neutral gas can be included in PIC methods. Generally, collisions reduce the real frequency and increase the damping of the waves; this can be shown theoretically and has been confirmed by the simulations in both the fluid and crystal limits. PIC methods also allow the background ions to be treated kinetically, which can be important if there is additional physics, such as flow between the dust and the plasma, that modifies the symmetry of the shielding cloud around each dust grain. Here we have shown that in the absence of flow, the simulations indicate that the dispersion properties of the waves are not modified to a significant degree, except perhaps at very long wavelengths, by kinetic ions. However, the simulations have a much higher overall level of fluctuations, which may lead to mode coupling and hence the long-wavelength modification of the spectrum.

While this study has concentrated on simple one-dimensional, periodic systems, actual dusty plasmas are fully three dimensional, or perhaps thin enough in one dimension that they are nearly two dimensional and usually aperiodic. In such situations and where the dust grains are relatively large and form into crystalline structures, MD simulations provide the best modeling method. If the grains are smaller and overall fluidlike dynamics are the goal of the simulation study, PIC methods with Boltzmann ions should be used. If there is relative flow between plasma and dust species, the interaction becomes more complex. In this case, some model for the interaction involving the wake produced by a dust grain in a flowing plasma [25,28] or treating the process through some sort of dipole force [47,48] could be used in both MD and PIC simulations. If possible, such calculations should be compared to PIC simulations with particle ions. The coupling of waves produced by flow in one direction to other low-frequency wave modes generated in the directions transverse to the flow may also require further modification of the interaction between dust grains in both the MD and PIC descriptions.

Experimentally, dusty plasma crystals are produced in low-density rf discharges, where the dust grains collect in traps above the electrodes [5,6,8]. In these traps, the downward gravitational force is balanced by the repulsive electrostatic force of negatively charged grains. There is also flow of plasma through the trap towards the electrode. Typically, the trap is only a few layers thick. In such a system, the excitation and detection of low-frequency waves in the flow direction is very difficult [49] and waves have usually been studied in the plane transverse to the flow [16]. In this case modification to the wave properties seen to be dominated by collisions rather than strongly coupled plasmas effects [16,26,50–52]. However, the study of waves in the flow direction may lead to a better understanding of wave generation and coupling in a three-dimensional system. Furthermore, it may give some information about the properties of the shielding provided by the background plasma [16] or about the size of the dust grains themselves [21]. In addition, since low-frequency waves are observed as the crystal melts [8], their study may also contribute to further understanding of the phase transition process. Moreover, since some experiments indicate that relatively large-amplitude waves can be generated [7,9], and other experiments show waves on strings of dust grains [53], simulations of these systems may say something about the nonlinear behavior of the waves.

ACKNOWLEDGMENTS

At Los Alamos, this work was supported by the Laboratory Directed Research and Development Program. At the University of California, San Diego, this work was supported by the U.S. Department of Energy under Grant No. DE-FG03-97ER54444 and by the U.S. Air Force under Grant No. F49620-95-1-0293.

[1] C. K. Goertz, Rev. Geophys. **27**, 271 (1989).
[2] D. A. Mendis and M. Rosenberg, Annu. Rev. Astron. Astrophys. **32**, 419 (1994).
[3] D. A. Mendis, in *Advances in Dusty Plasmas*, edited by P. K. Shukla, D. A. Mendis, and T. Desai (World Scientific, Singapore, 1997), p. 3.
[4] D. A. Mendis, H. L. F. Houpis, and J. R. Hill, J. Geophys. Res. **87**, 3449 (1982).
[5] J. H. Chu and L. I, Phys. Rev. Lett. **72**, 4009 (1994).
[6] H. Thomas, G. E. Morfill, V. Demmel, J. Goree, B. Feuerbacher, and D. Mohlmann, Phys. Rev. Lett. **73**, 652 (1994).
[7] A. Barkan, R. L. Merlino, and N. D'Angelo, Phys. Plasmas **2**, 3563 (1995).
[8] A. Melzer, A. Homann, and A. Piel, Phys. Rev. E **53**, 2757 (1996).
[9] R. L. Merlino, A. Barkan, C. Thompson, and N. D'Angelo, Phys. Plasmas **5**, 1607 (1998).
[10] F. Y. Huang, H. H. Hwang, and M. J. Kushner, J. Vac. Sci. Technol. A **14**, 562 (1996).
[11] N. N. Rao, J. Plasma Phys. **49**, 375 (1993).
[12] M. Rosenberg, in *Physics of Dusty Plasmas*, edited by P. K. Shukla, D. A. Mendis, and V. W. Chow (World Scientific, Singapore, 1996), p. 129.
[13] F. Verheest, Space Sci. Rev. **77**, 267 (1996).
[14] N. N. Rao, P. K. Shukla, and M. Y. Yu, Planet. Space Sci. **38**, 543 (1990).
[15] N. D'Angelo, Planet. Space Sci. **38**, 1143 (1990).
[16] J. B. Pieper and J. Goree, Phys. Rev. Lett. **77**, 3137 (1996).
[17] C. Thompson, A. Barkan, N. D'Angelo, and R. L. Merlino, Phys. Plasmas **4**, 2331 (1997).
[18] M. Rosenberg, Planet. Space Sci. **41**, 229 (1993).
[19] D. Winske, S. P. Gary, M. E. Jones, M. Rosenberg, V. W. Chow, and D. A. Mendis, Geophys. Res. Lett. **22**, 2069 (1995).
[20] D. H. Van Winkle and C. A. Murray, J. Chem. Phys. **89**, 3885 (1988).
[21] U. Kortshagen, Appl. Phys. Lett. **71**, 208 (1997).
[22] M. Zuzic, H. Thomas, and G. E. Morfill, J. Vac. Sci. Technol. A **14**, 496 (1996).

[23] F. Melandso, Phys. Plasmas **3**, 3890 (1996).
[24] F. Melandso, Phys. Rev. E **55**, 7495 (1997).
[25] S. V. Vladimirov, P. V. Shevchenko, and N. F. Cramer, Phys. Plasmas **5**, 4 (1998).
[26] M. Rosenberg and G. Kalman, Phys. Rev. E **56**, 7166 (1997).
[27] M. S. Murillo, Phys. Plasmas **5**, 3116 (1998).
[28] F. Melandso and J. Goree, J. Vac. Sci. Technol. A **14**, 511 (1996).
[29] J. E. Hammerberg, B. L. Holian, and R. Ravelo, Phys. Rev. E **50**, 1372 (1994).
[30] H. Totsuji, T. Kishimoto, and T. Totsuji, Phys. Rev. Lett. **78**, 3113 (1997).
[31] H. H. Hwang and M. J. Kushner, J. Appl. Phys. **82**, 2106 (1997).
[32] J. E. Hammerberg, B. L. Holian, G. Lapenta, M. S. Murillo, W. R. Shanahan, and D. Winske, in *Proceedings of the International Conference on Strongly Coupled Coulomb Systems*, edited by G. Kalman (Plenum, New York, 1998).
[33] D. Winske, M. S. Murillo, G. S. Selwyn, and M. Rosenberg, Bull. Am. Phys. Soc. **42**, 1825 (1997).
[34] C. K. Birdsall and A. B. Langdon, *Plasma Physics via Computer Simulation* (McGraw-Hill, New York, 1985).
[35] N. Otani and A. Bhattacharjee, Phys. Rev. Lett. **78**, 1468 (1997).
[36] O. Ishihara and S. V. Vladimirov, Phys. Rev. E **57**, 3392 (1998).
[37] N. D'Angelo and R. L. Merlino, Planet. Space Sci. **44**, 1593 (1996).
[38] P. K. Shukla, G. T. Birk, and G. Morfill, Phys. Scr. **56**, 299 (1997).
[39] R. Bharuthram and T. Pather, Planet. Space Sci. **44**, 137 (1996).
[40] D. Winske and M. Rosenberg, IEEE Trans. Plasma Sci. **26**, 92 (1998).
[41] X. H. Zheng and J. C. Earnshaw, Phys. Rev. Lett. **75**, 4214 (1995).
[42] S. J. Choi and M. J. Kushner, IEEE Trans. Plasma Sci. **22**, 138 (1994).
[43] G. Lapenta, Phys. Rev. Lett. **75**, 4409 (1995).
[44] D. S. Lemons, J. Lackman, M. E. Jones, and D. Winske, Phys. Rev. E **52**, 6855 (1995).
[45] M. E. Jones, D. S. Lemons, R. J. Mason, V. A. Thomas, and D. Winske, J. Comput. Phys. **123**, 169 (1996).
[46] D. Winske, M. S. Murillo, and M. Rosenberg, in *Physics of Dusty Plasmas*, edited by M. Horanyi, S. Robertson, and B. Walch, AIP Conf. Proc. 446 (AIP, Woodbury, NY, 1998), p. 101.
[47] H. C. Lee and D. Y. Chen, Phys. Rev. E **56**, 4596 (1997).
[48] J. E. Hammerberg, B. L. Holian, M. S. Murillo, and D. Winske, in *Physics of Dusty Plasmas* (Ref. [46]), p. 257.
[49] M. Rosenberg, J. Vac. Sci. Technol. A **14**, 631 (1996).
[50] X. Wang and A. Bhattacharjee, Phys. Plasmas **4**, 3759 (1997).
[51] P. K. Kaw and A. Sen, Phys. Plasmas **5**, 3552 (1998).
[52] M. Rosenberg and G. Kalman, in *Physics of Dusty Plasmas* (Ref. [46]), p. 135.
[53] A. Homann, A. Melzer, S. Peters, and A. Piel, Phys. Rev. E **56**, 7138 (1997).